Supplementary Material of

Reconstructing Younger Dryas Ground Temperature and Snow Thickness from Cave Deposits

5   Paul Töchterle et al.

Correspondence to: Paul Töchterle (paul.toechterle@uibk.ac.at)

Includes:

- Figures S1 to S7
10   - Table S1
- Isochrons
- References
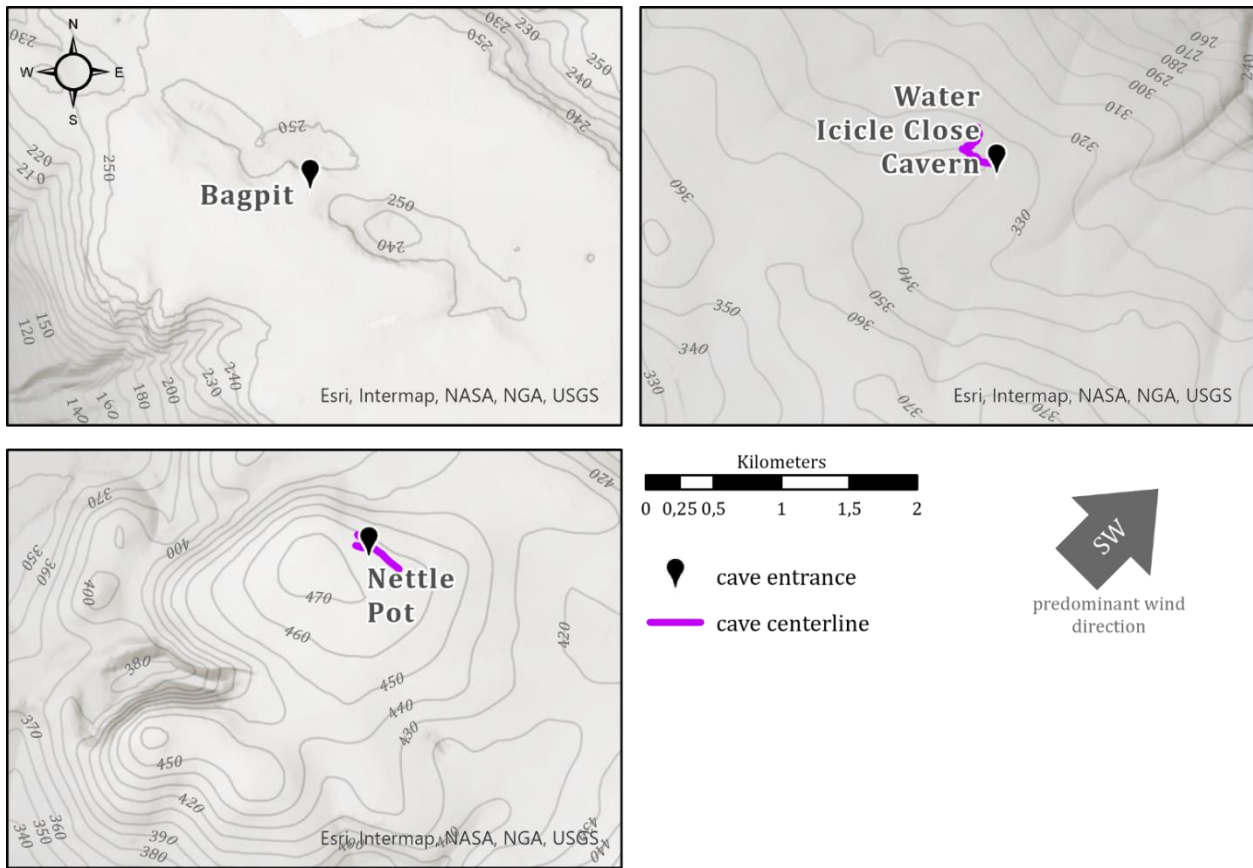
15 **Fig. S1: Topographical maps (scale 1:50 000) of the three cave sites with 10 m contour lines. The locations of cave entrances is marked by a black pin symbol. Centerlines of the cave passages are shown in purple. The caves are located leeward of the predominant south-westerly wind direction as inferred from modern re-analysis data (ERA5 monthly from 1990 to 2020, *54*).**

A) Water Icicle Close Cavern (WIC)

plan view

100 m

N

profile view

Ω
Entrance shaft (32m)

B) Bagpit (BGP)

plan view

Ω

profile view

Ω   10 m

o sampled CCCs

C) Nettle Pot (NTL)

plan view

Ω

100 m

profile view

Ω
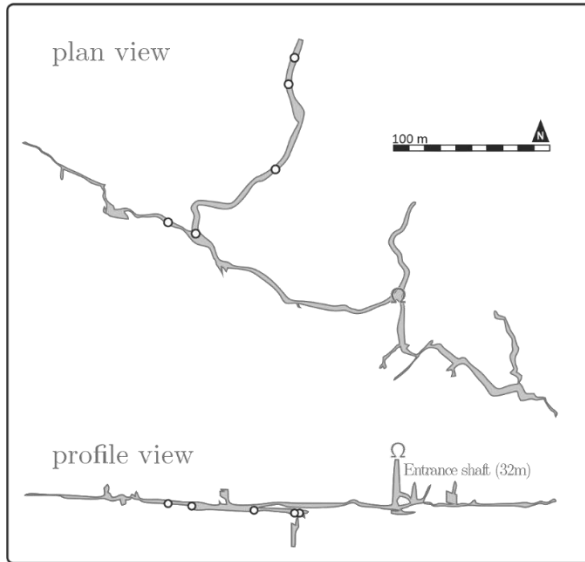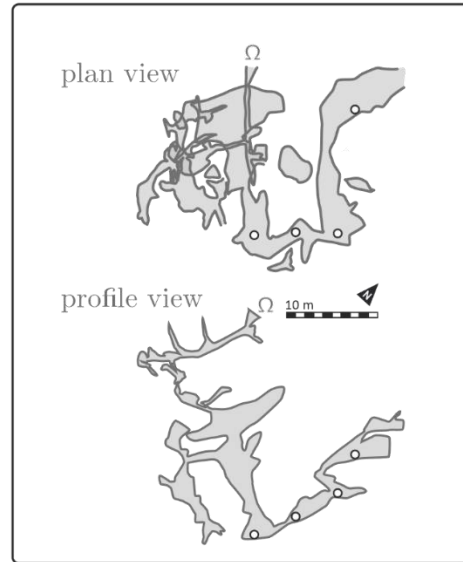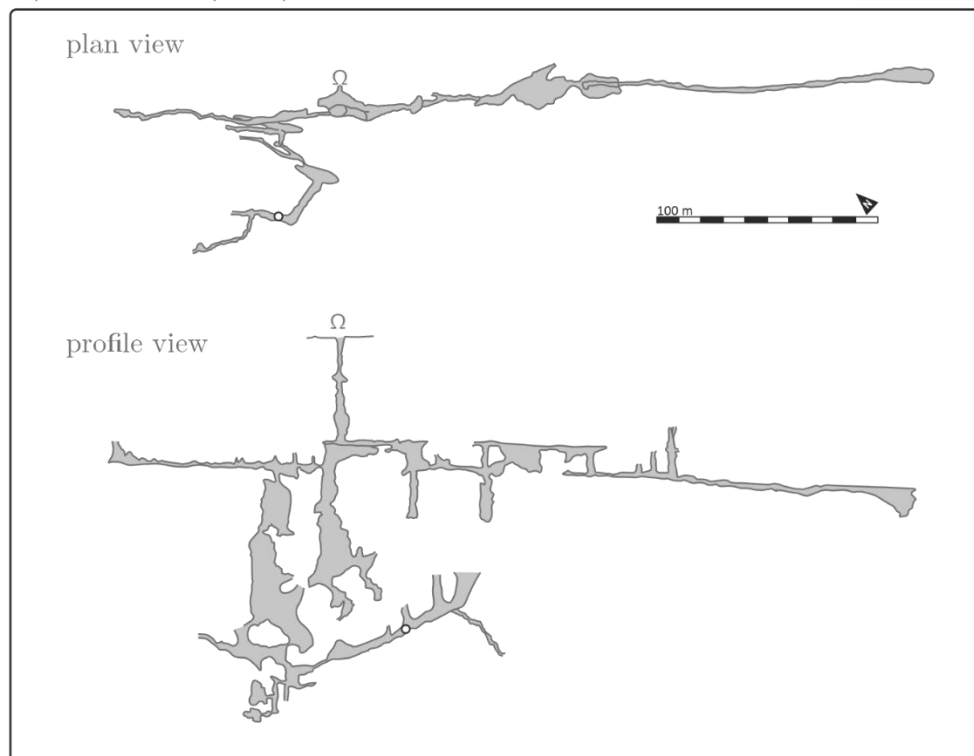
Fig. S2: Cave maps of (A) Water Icicle Close Cavern, (B) Bagpit and (C) Nettle Pot. Locations of the sampled CCC sites are marked by white dots.

20
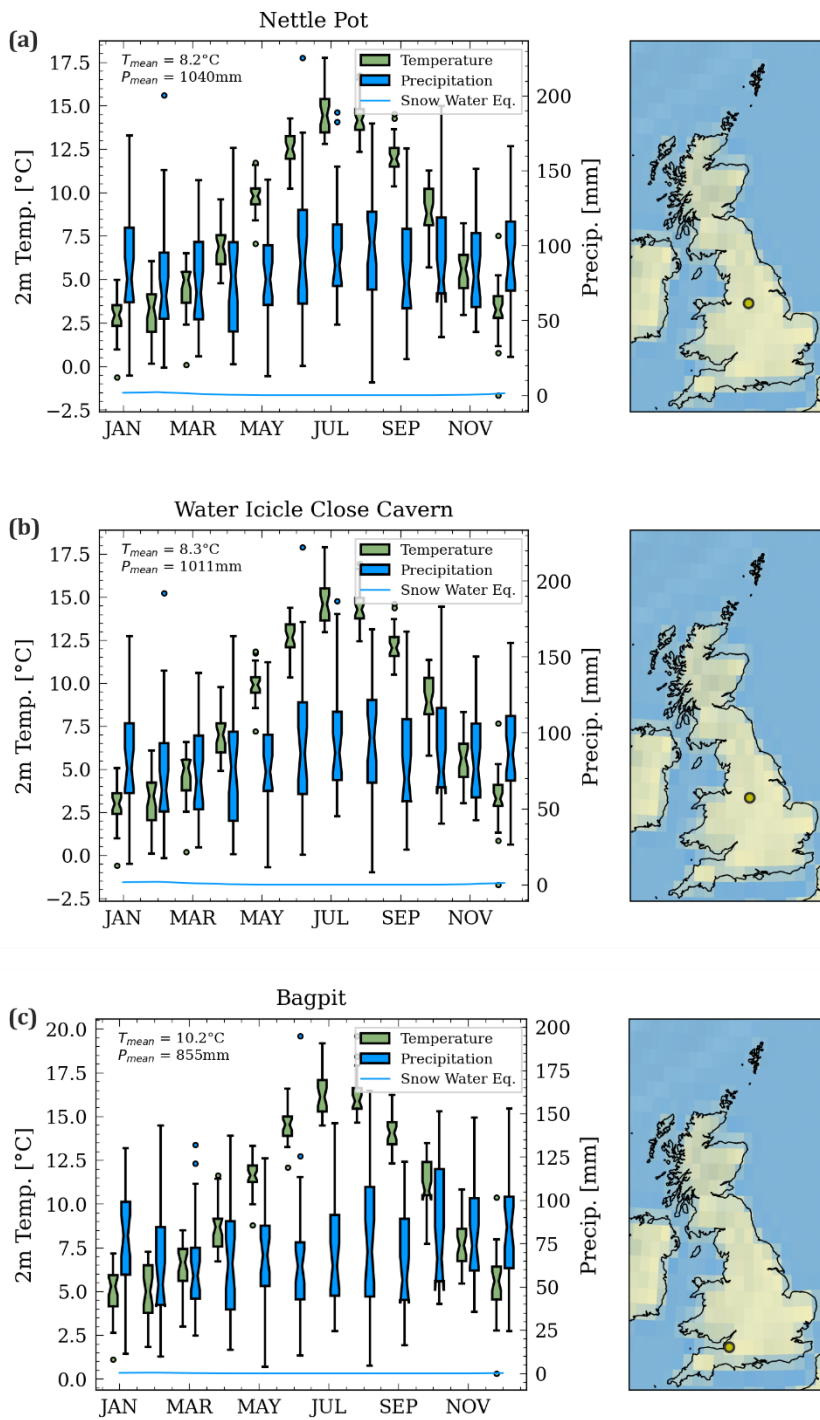
Fig. S3: Climate diagrams for the three studied cave sites based on reanalysis data between 1990 and 2020 (ERA5 monthly, Muñoz-Sabater, 2019).
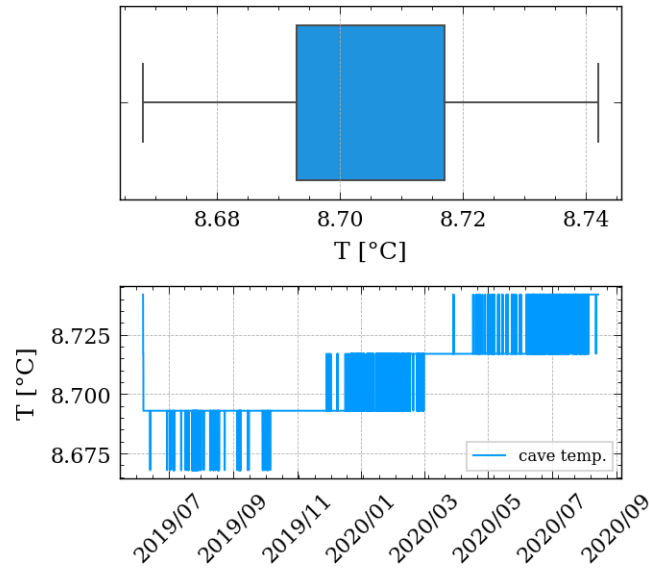
25

Fig. S4: Cave air temperature monitoring of Water Icicle Close Cavern. The lower panel shows the time series of temperature over the monitoring period. The increase in temperature is likely the result of instrument drift. The upper panel shows a boxplot of the same dataset.
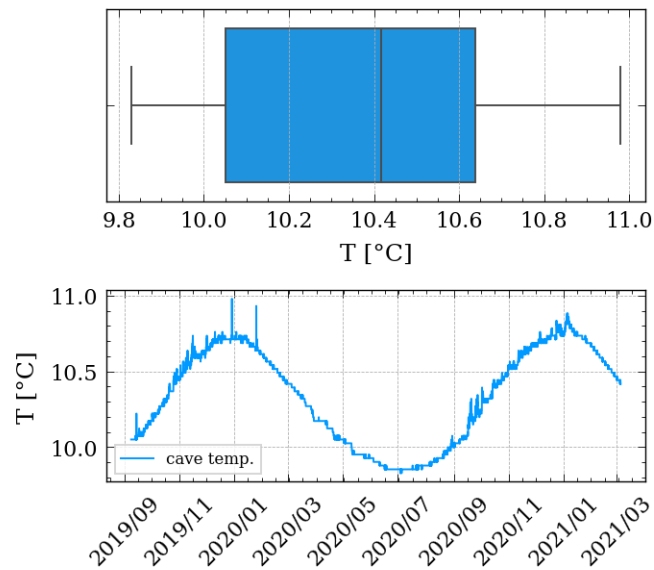
30   **Fig. S5: Cave air temperature monitoring of Bagpit. The lower panel shows the time series of temperature over the monitoring period. The cave temperature follows a seasonal cycle with that is attenuated and offset by approx. six months from the outside atmospheric cycle. Small positive excursions on the rising limb of the curve are likely caused by advective heat flux from percolating drip water. The upper panel shows a boxplot of the same dataset.**

single grains
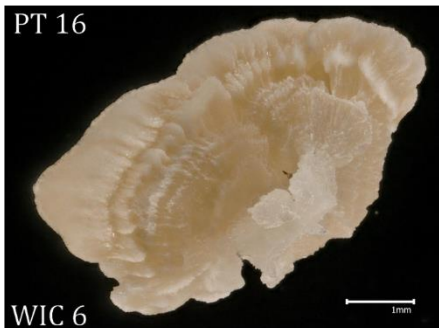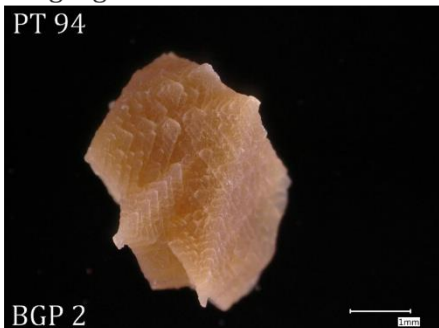
aggregates
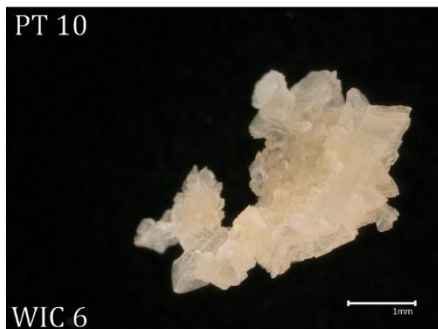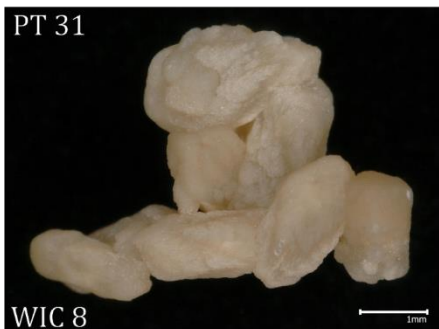
multigrain aliquots

35 **Fig. S6: Microscopic images of selected CCC samples. The sample codes refer to the respective lab and sample IDs in table 1, table S1 and the main text.**
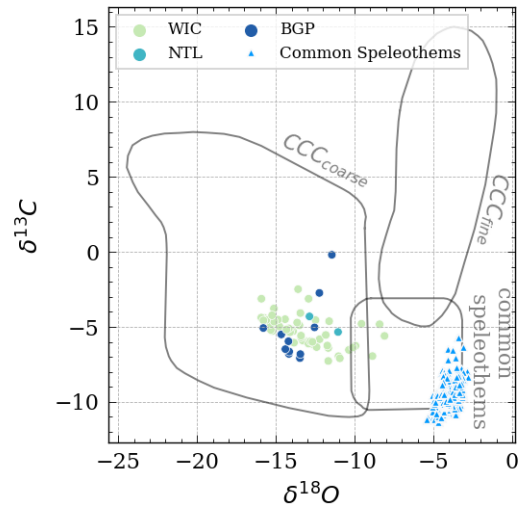
Fig. S7: Stable C and O isotope data for CCC samples analysed in this study (circles) and common speleothems from Water Icicle Close Cavern (triangles) (Gunn et al., 2020) in comparison to Central European reference values (grey outlines) in (Žák et al., 2018). The CCC samples analysed in this study broadly fall within the range of the reference values, albeit with δ¹⁸O values at the higher end and δ¹³C values at the lower end. Less negative δ¹⁸O can be explained by the fact that the study area is situated closer to the moisture source than the reference data.

40

Isochron	Lab ID	^{238}U [ng g^{-1}]		^{232}Th [pg g^{-1}]		(^{230}Th/^{232}Th) [atomic *10^{-6}]		δ^{234}U*		(^{230}Th/^{238}U) [activity *10^{-3}]	
BGP1	PT96	2199	± 6	156567	± 3168	41	± 1	362.9	± 3.1	175.1	± 0.8
	PT129	2343	± 3	41225	± 826	150	± 3	364.3	± 1.7	160.2	± 0.4
	PT97	2238	± 4	36920	± 741	161	± 3	365.7	± 1.9	160.8	± 0.5
	PT95	2264	± 6	35111	± 710	170	± 3	364.2	± 3.1	159.6	± 0.6
	PT117	2324	± 4	16695	± 335	357	± 7	363.2	± 2.0	155.7	± 0.6
	PT118	2264	± 3	12912	± 259	449	± 9	362.9	± 1.8	155.3	± 0.5
	PT130	2293	± 2	44394	± 889	137	± 3	360.1	± 1.4	161.0	± 0.3
BGP2	PT54	1643	± 1	10334	± 207	368	± 7	253.2	± 1.6	140.5	± 0.4
	PT120	1693	± 2	25024	± 501	158	± 3	252.6	± 1.6	141.9	± 0.3
	PT121	1652	± 2	17019	± 341	227	± 5	254.7	± 1.6	141.9	± 0.6
	PT119	1618	± 2	14790	± 296	255	± 5	251.9	± 1.6	141.4	± 0.6
	PT94	1898	± 2	5894	± 118	749	± 15	252.1	± 1.6	141.2	± 0.3
	PT122	1508	± 2	18375	± 368	192	± 4	251.4	± 1.7	141.6	± 0.3
	PT123	1823	± 2	10804	± 217	389	± 8	253.6	± 1.6	139.7	± 0.6
BGP3	PT113	2117	± 3	49180	± 986	112	± 2	237.1	± 1.6	158.1	± 0.3
	PT114	2158	± 3	32236	± 646	169	± 3	240.9	± 1.6	153.3	± 0.3
	PT92	2081	± 3	23092	± 463	221	± 4	241.0	± 1.8	149.0	± 0.5
BGP4	PT87	2440	± 4	60564	± 1214	111	± 2	491.1	± 1.9	167.5	± 0.5
	PT127	2389	± 4	20264	± 407	312	± 6	475.3	± 3.0	160.4	± 0.8
	PT88	2196	± 4	15839	± 318	365	± 7	458.4	± 2.2	159.5	± 0.4
	PT128	2374	± 2	9844	± 198	627	± 13	456.3	± 1.7	157.6	± 0.4
NTL1	PT86	5125	± 13	36963	± 745	485	± 10	952.5	± 2.2	211.9	± 0.6
	PT134	5652	± 10	21791	± 437	892	± 18	962.8	± 2.5	208.5	± 0.5
	PT133	5147	± 12	19672	± 396	894	± 18	960.0	± 3.4	207.2	± 0.7
	PT85	5049	± 9	11083	± 223	1545	± 31	957.7	± 1.8	205.6	± 0.5
	PT132	5773	± 7	11547	± 232	1683	± 34	964.0	± 2.0	204.2	± 0.5
WIC2	PT65	1479	± 1	4742	± 95	914	± 19	551.2	± 1.9	177.7	± 0.5
	PT136	1575	± 2	20416	± 409	248	± 5	539.8	± 1.8	194.7	± 0.4
	PT135	1484	± 2	15116	± 303	309	± 6	542.7	± 1.7	190.8	± 0.5
WIC5	PT84	1499	± 2	6499	± 130	628	± 13	549.2	± 2.1	165.1	± 0.3
	PT143	1120	± 1	6559	± 131	472	± 10	557.4	± 2.1	167.6	± 0.4
	PT144	1360	± 2	7633	± 153	491	± 10	536.8	± 1.9	167.2	± 0.5
WIC6	PT10	3340	± 5	19264	± 387	630	± 13	1034.4	± 1.9	220.5	± 0.6
	PT11	3147	± 4	10802	± 217	1042	± 21	1038.0	± 2.0	216.9	± 0.4
	PT09	3010	± 4	6218	± 125	1706	± 34	1038.9	± 2.2	213.7	± 0.4
	PT17	1758	± 2	1884	± 38	3215	± 65	1042.3	± 1.6	209.0	± 0.3
	PT16	1703	± 2	1074	± 22	5459	± 110	1041.5	± 2.3	208.9	± 0.3
	PT15	1707	± 2	981	± 20	5994	± 121	1039.3	± 2.7	209.0	± 0.4
WIC8	PT34	1087	± 1	54301	± 1088	69	± 1	487.8	± 2.0	210.0	± 0.4
	PT32	1072	± 2	52299	± 1049	72	± 1	490.9	± 2.4	211.7	± 0.8
	PT35	1198	± 2	36337	± 730	104	± 2	488.0	± 3.0	191.7	± 0.7
	PT31	1092	± 1	30804	± 617	108	± 2	492.7	± 1.9	185.3	± 0.4
	PT30	1035	± 1	25456	± 510	122	± 2	491.6	± 1.7	182.3	± 0.6
	PT29	1680	± 3	6514	± 131	675	± 14	492.8	± 2.5	158.9	± 0.4
	PT28	1487	± 1	5510	± 110	718	± 14	488.7	± 1.5	161.4	± 0.2
	PT27	1466	± 1	4733	± 95	808	± 16	489.6	± 2.0	158.3	± 0.3
WIC9	PT07	1640	± 2	5183	± 104	866	± 18	492.4	± 1.6	166.1	± 0.5
	PT08	1574	± 1	3066	± 61	1372	± 28	491.4	± 1.8	162.1	± 0.3
	PT140	1518	± 2	35630	± 714	135	± 3	485.7	± 1.9	192.9	± 0.5
	PT141	1564	± 2	27773	± 557	169	± 3	484.5	± 1.9	181.7	± 0.4
	PT139	1634	± 2	20501	± 411	237	± 5	486.3	± 1.7	180.4	± 0.4

Table S1: Results of individual U/Th analyses on 51 aliquots of CCC samples from the three studied caves. The first column denotes the identifier of the respective CCC occurrence and isochron in table 1 of the main text. Uncertainties are reported at a 2σ level.

45 Isochrons

The following plots show the 3D ^{230}Th/U isochrons for each of the presented CCC deposits, based on the individual analyses from table S1. Depicted are the projections in the ^{232}Th/^{238}U vs. ^{234}U/^{238}U and ^{232}Th/^{238}U vs. ^{230}Th/^{238}U planes (Ludwig and Titterington, 1994). The least-squares linear regression (blue line) of the depicted dataset is shown with the 95 % confidence interval (shaded area) of the regression based on a bootstrap (n=1000). Regression metrics are provided in table 1 of the main 50 text.

BGP 1
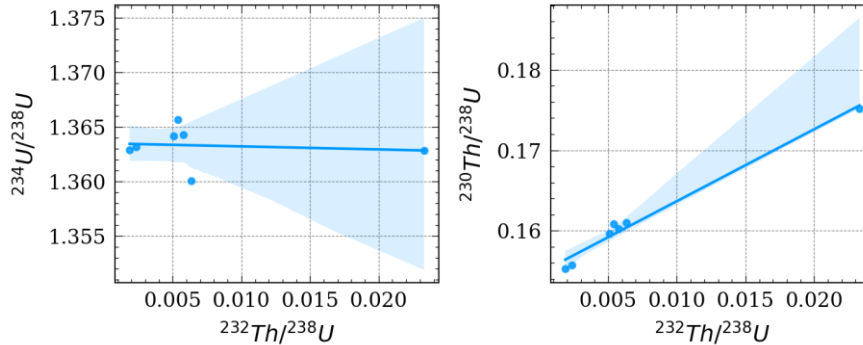
BGP 2
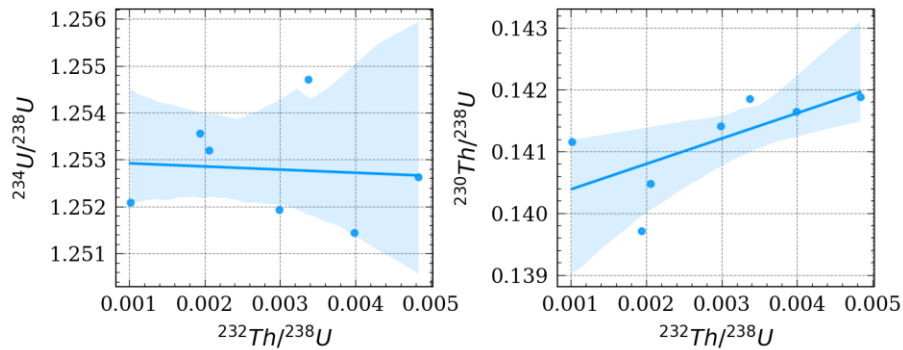
BGP 3
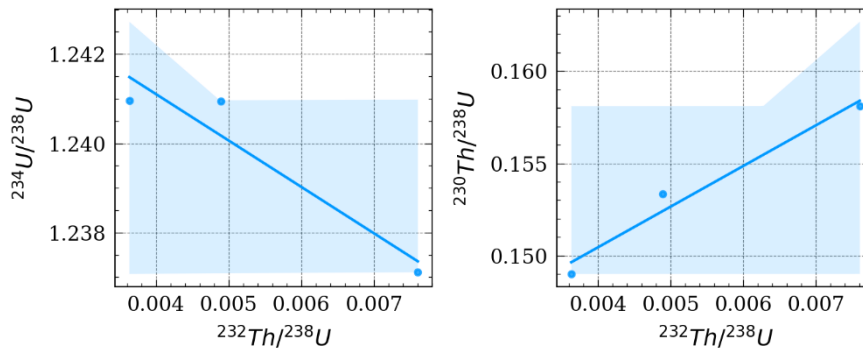
BGP 4
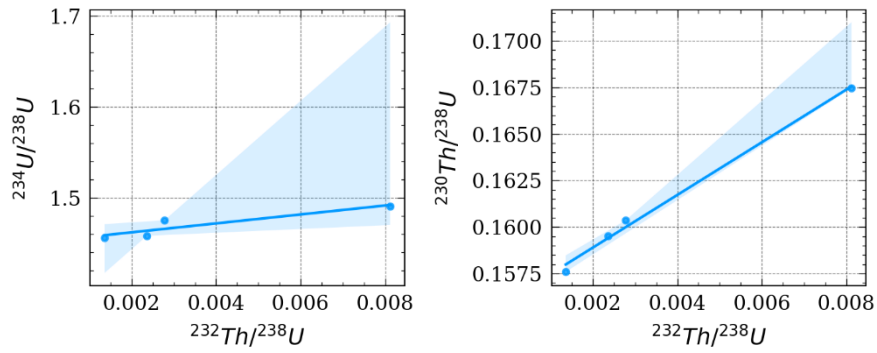
NTL 1
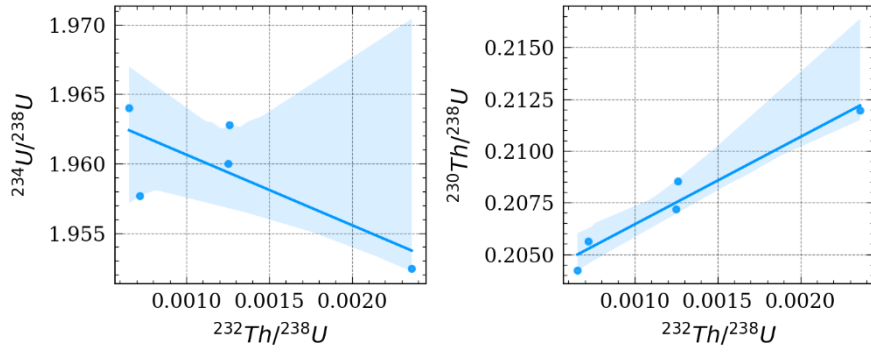
WIC 2
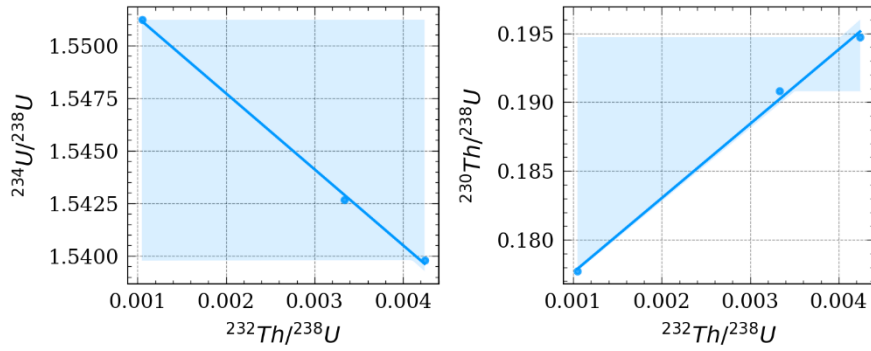
WIC 5
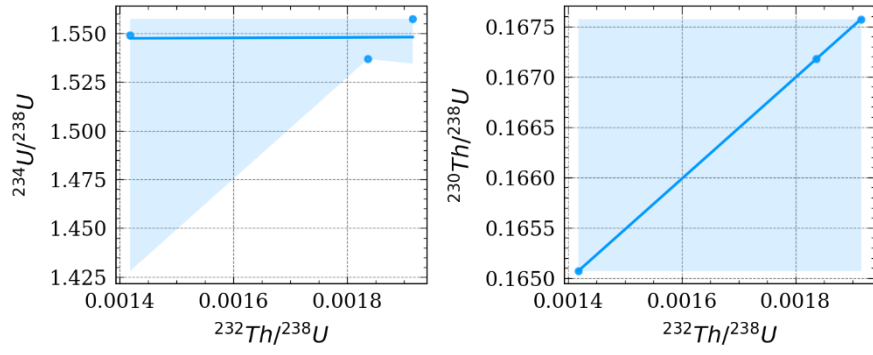
WIC 6
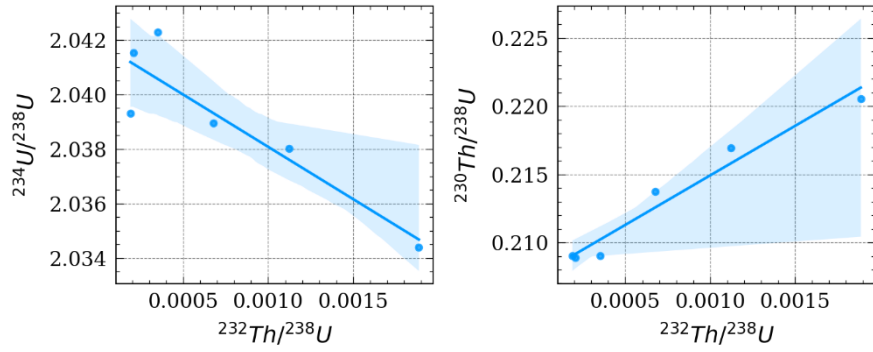
WIC 8
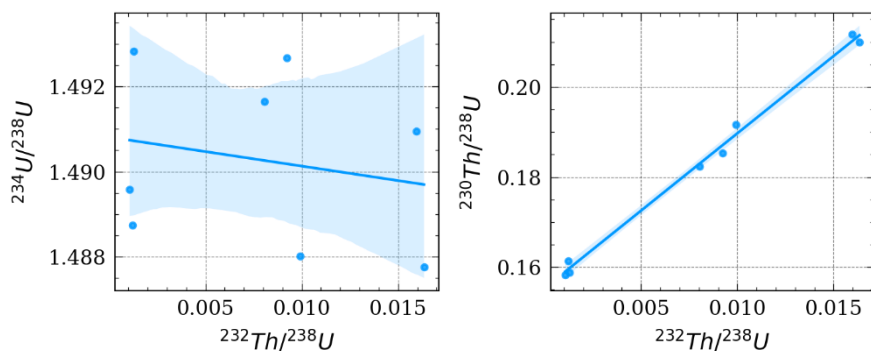
WIC 9
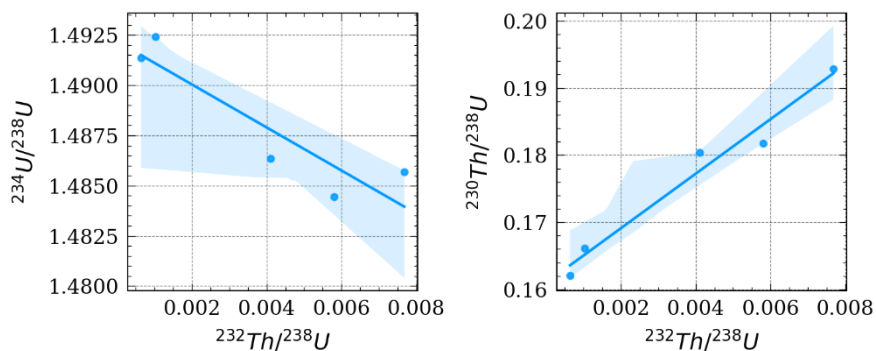
References

Gunn, J., Fairchild, I. J., Moseley, G. E., Töchterle, P., Ashley, K. E., Hellstrom, J., and Edwards, R. L.: Palaeoenvironments in the central White Peak District (Derbyshire, UK): evidence from Water Icicle Close Cavern, Cave Karst Sci., 47, 153–168, 2020.

Ludwig, K. R. and Titterington, D. M.: Calculation of 230^{Th}/U isochrons, ages, and errors, Geochim. Cosmochim. Ac., 58, 5031–5042, https://doi.org/10.1016/0016-7037(94)90229-1, 1994.

Muñoz-Sabater, J.: ERA5-Land monthly averaged data from 1981 to present, 2019.

Žák, K., Onac, B. P., Kadebskaya, O., Filippi, M., Dublyansky, Y., and Luetscher, M.: Cryogenic Mineral Formation in Caves, in: Ice caves, edited by: Perşoiu, A. and Lauritzen, S.-E., Elsevier, Amsterdam, Oxford, Cambridge, Mass., 2018.

60

65